Front. Struct. Civ. Eng. 2024, 18(5): 716–730
https://doi.org/10.1007/s11709-024-1053-7

RESEARCH ARTICLE

Research on an innovative structure of an open-ribbed steel–ultra-high performance concrete composite bridge deck

Xudong SHAO[a*], Xuan SUN[a], Deqiang ZOU[b], Junhui CAO[a], Chuanqi YANG[a]

[a] *School of Civil Engineering, Hunan University, Key Laboratory for Wind and Bridge Engineering of Hunan Province, Changsha 410082, China*

[b] *China Construction Fifth Engineering Division Co., Ltd., Changsha 410004, China*

[*] *Corresponding author. E-mail: shaoxd@hnu.edu.cn*

ABSTRACT To completely solve the problem of fatigue cracking issue of orthotropic steel bridge decks (OSDs), the authors proposed a steel–ultra-high performance concrete (UHPC) lightweight composite deck (LWCD) with closed ribs in 2010. Based on the successful application of that LWCD, an adaptation incorporating an innovative composite deck structure, i.e., the hot-rolled section steel–UHPC composite deck with open ribs (SSD) is proposed in this paper, aiming to simplify the fabrication process as well as to reduce the cost of LWCD. Based on a long-span cable-stayed bridge, a design scheme is proposed and is compared with the conventional OSD scheme. Further, a finite element (FE) calculation is conducted to reflect both the global and local behavior of the SSD scheme, and it is found that the peaked stresses in the SSD components are less than the corresponding allowable values. A static test is performed for an SSD strip specimen to understand the anti-cracking behavior of the UHPC layer under negative bending moments. The static test results indicate that the UHPC layer exhibited a satisfactory tensile toughness, the UHPC tensile strength obtained from the test is 1.8 times the calculated stress by the FE model of the real bridge. In addition, the fatigue stresses of typical fatigue-prone details in the SSD are calculated and evaluated, and the influences of key design parameters on the fatigue performance of the SSD are analyzed. According to the fatigue results, the peaked stress ranges for all of the 10 fatigue-prone details are within the corresponding constant amplitude fatigue limits. Then a fatigue test is carried out for another SSD strip specimen to explore the fatigue behavior of the fillet weld between the longitudinal and transverse ribs. The specimen failed at the fillet weld after equivalent 47.5 million cycles of loading under the design fatigue stress range, indicating that the fatigue performance of the SSD could meet the fatigue design requirement. Theoretical calculations and experiments provide a basis for the promotion and application of this structure in bridge engineering.

KEYWORDS steel–ultra-high performance concrete composite deck, open rib, strip model test, static and fatigue performance, orthotropic steel deck

1 Introduction

Orthotropic steel bridge decks (OSDs) are widely used in steel bridges because of advantages such as light self-weight, high capacity, and convenience in construction, and a typical OSD consists of a steel deck plate, longitudinal stiffeners, and diaphragms [1]. However, as OSDs generally have complicated configurations, many OSDs have experienced severe fatigue cracking problems, under wheel loads, within 10–20 years [2–5], which is much less than the design service life of bridges (i.e., 100 years).

The rib-to-deck (RD) plate joint is one of the most critical fatigue-prone details in OSDs [4,6–8]. Currently, the commonly used methods to address the issue include increasing the thickness of the steel deck plate or the penetration rate of the RD welded joints [7,9,10], welding the U-shaped ribs from both the outer and inner sides at

Article history: Received Apr 15, 2023; Accepted Aug 11, 2023

the connections to form the double-sided welds [10,11], and improving the thickness of U-shaped ribs at the ends near the RD joints [12,13] to provide a greater weld thickness. Although the above methods can alleviate the fatigue cracking issue of the RD joints to certain extents, high stress ranges generated by local wheel loads still exist at the RD joints, implying that there is still a high cracking risk within the service life of OSD bridges.

The rib-to-floor (RF) beam joint is the most complex fatigue-prone detail in OSDs [3,14,15]. Currently, the methods available include refining the geometric configurations of the cutouts in the diaphragms to reduce the high stress concentration [16–18], using bulkhead installed inside the U-rib at the floor beam or cancel the cutouts to improve the in-plane stiffness of the RF joints [19–22], refining the configuration of longitudinal ribs such as adoption of open ribs or large-sized U-ribs to improve the fatigue strength [23–25], etc. However, the above methods cannot simplify the complex connection structure at the RF joints, so the high secondary deformation and stress at the connections cannot be avoided. In other words, currently there is no widely recognized method to eliminate the fatigue cracking issues at the RF joints.

Thus, to solve the fatigue cracking issue of OSDs, the authors propose a new structure, i.e., the steel–ultra-high performance concrete (UHPC) lightweight composite deck (LWCD) with closed ribs, created by laying a thin layer of UHPC on the top of the steel deck plate [26–32]. UHPC is an advanced cement-based material developed in 1993, which possesses ultra-high toughness, ultra-high strength and ultra-high durability [33–35]. A series of investigations have been carried out on the LWCD, including the fatigue resistance [26–29,36–39], basic mechanical properties of the UHPC layer in the composite deck [30,31,39,40], and ant-shearing performance of the headed stud connectors at the steel–UHPC interface [41,42]. Research and applications have shown that the LWCD can significantly reduce the fatigue stresses of the steel deck plate and hence completely solve the fatigue cracking issue at the RD joint. This new technology has now been widely used in both newly constructed bridges and in-service bridges [29,32,43,44].

Considering that the UHPC layer can substantially increase the local bending stiffness of the steel deck plate [26], the OSD in the LWCD can be further simplified. Thus, in this paper, an innovative steel–UHPC composite deck composed of hot-rolled section steel–UHPC composite deck with open ribs (SSD) is proposed. The new bridge deck structure can significantly simplify the bridge deck structure and reduce the construction effort, and has the potential to completely address the fatigue cracking issue with conventional OSDs and to simplify the construction process.

In this paper, the behaviors of the OSD and SSD are fully compared basing on a long-span cable-stayed bridge. The response of the SSD is analyzed through both global and local finite element (FE) analyses. Further, a static experimental test is carried out for an SSD strip specimen and a calculation method is proposed to evaluate the cracking resistance of UHPC under negative bending moments. In addition, the stress ranges for the fatigue-prone details under vehicle load of different steel decks are calculated and compared. On the basis of the FE analyses, and the influence of the critical design parameters of the SSD, the fatigue resistance is discussed. Finally, a fatigue test is conducted for the welded connection in the SSD strip specimen to verify the structural feasibility and safety of the proposed scheme.

2 Structural concept of hot-rolled section steel–ultra-high performance concrete composite deck with open ribs

OSDs can be generally divided into two types: open-ribbed OSDs and close-ribbed OSDs [1]. Generally, open ribs (Figs. 1(a)–1(c)) are easy to splice in the field and simple to fabricate and maintain. But the transverse stress distribution of open ribs is not very efficient in comparison to that of closed ribs. U-shape rib (Fig. 1(d)) is the most common form of closed rib. Compared with the open ribs, the close rib has much higher flexural and torsional rigidity and better compression stability. But, the complex geometric structure of the close rib makes the OSD more susceptible to fatigue.

The OSDs generally suffers from a common disease, the fatigue cracking of the steel, which becomes the biggest limiting factor in the application of OSDs. The LWCD (Fig. 2) proposed by the authors has been proven to be a very effective solution in real bridge applications. Figure 3 shows the two different types of deck plates, the

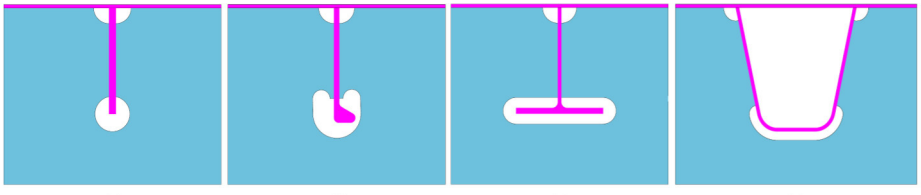

Fig. 1 OSD with open ribs and closed ribs: (a) flat; (b) bulb; (c) T-shape; (d) U-shape.

flexural stiffness of composite deck of LWCD is 24.7 times that of the OSD by calculation. Since the rigidity of the deck has been greatly improved, it is unnecessary to adopt closed ribs to improve the local rigidity. Therefore, open ribs with a simpler structure can be used instead, and the connection structure of the longitudinal ribs and the floorbeam can be optimized to simplify processing.

Based on the successful application of the LWCD, the authors further proposed the SSD, as shown in Fig. 4. The specific construction process is as follows: steel deck plate is placed on the bottom, and the T-shaped steel sections are welded as longitudinal ribs. Further T-shaped steel sections are orthogonally stacked, as transverse ribs, above the longitudinal ribs, and the longitudinal and transverse ribs are connected by transverse fillet welds (Fig. 4(b)). Turning over the steel deck unit, the webs of the transverse T-shaped ribs are positioned in line with the floorbeams of the girder, and are connected by the butt welds at the webs. Finally, head studs are welded on the steel deck plate, longitudinal and transverse reinforcement are arranged, and UHPC is cast-in-place.

The advantages of the new composite bridge deck structure can be attributed to the following factors. First, the use of the UHPC layer can significantly improve the local stiffness of the bridge deck and reduce the stresses in the RD joints. Second, the configuration for the connection between the longitudinal and transversal ribs is simple and this can further eliminate the fatigue

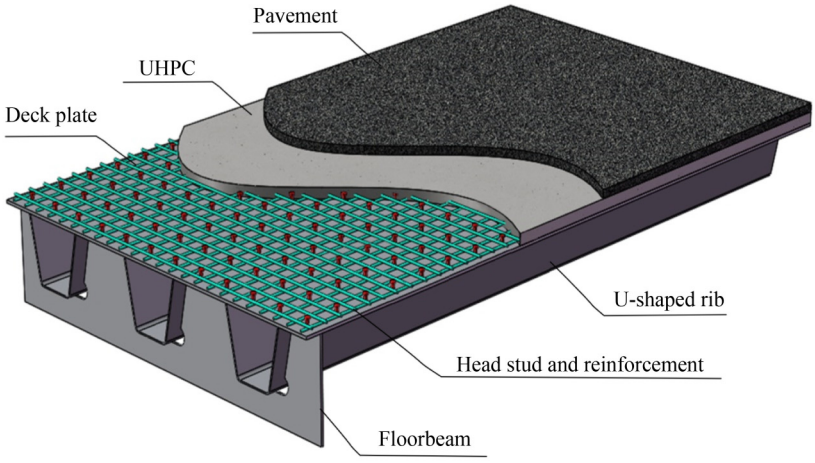

Fig. 2 Schematic drawings of the LWCD.

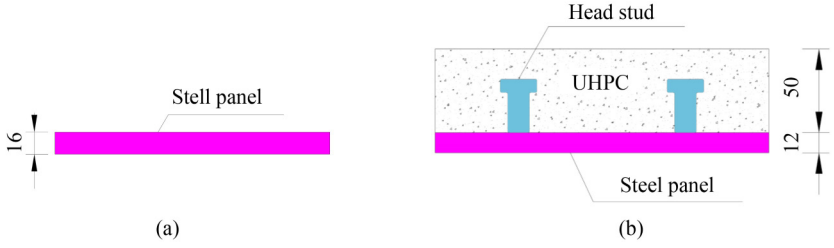

Fig. 3 Comparison of two types of bridge deck: (a) steel deck plate; (b) steel–UHPC composite deck.

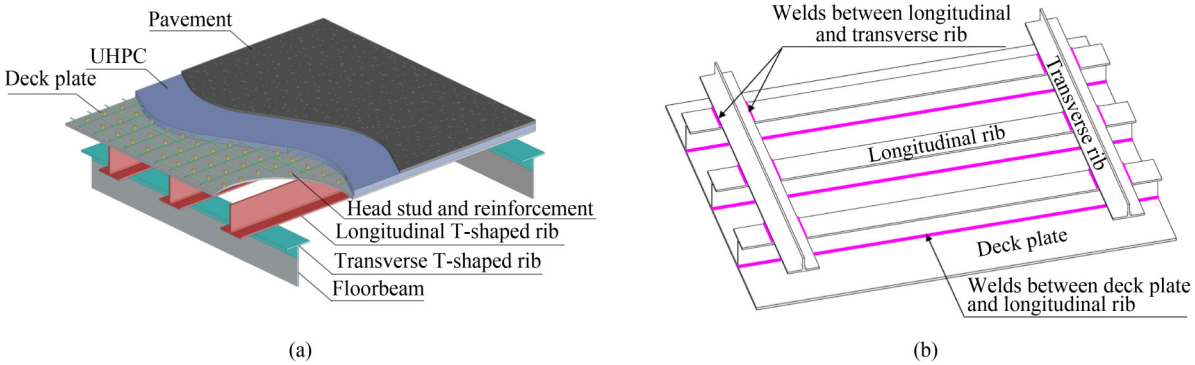

Fig. 4 Schematic drawings of the SSD and welds connection: (a) schematic drawing of the SSD; (b) deck unit and welds connection.

cracking issue of the RF joints. Thirdly, section steel can be purchased directly on the market without additional processing, thus reducing the construction effort and costs.

3 Application and comparison of hot-rolled section steel–ultra-high performance concrete composite deck with open ribs

3.1 Background project introduction

Based on a large span cable-stayed bridge, the application of SSD is studied and compared here. The bridge is a semi-floating system cable-stayed bridge with two towers and two cable planes, whose span arrangement is (210 + 658 + 240) m with a total length of 1108 m. The elevation layout of the main bridge is shown in Fig. 5. The girder contains two flat streamlined side boxes, which are connected by the cross-beam in the middle, with a total width of 51.85 m (including the wind fairing), and the depth of the girder at the center line is 3.8 m. The cables are arranged on the outer webs on both side box with a standard spacing of 15.0 m. For the original design of the steel girder, the OSD scheme (Fig. 6(a)) is adopted, with 16 mm steel deck plate + 80 mm special asphalt pavement, the longitudinal ribs are 8 mm U-shape ribs with 600 mm lateral spacing.

After optimization, an SSD scheme (Fig. 6(b)) is adopted, with 40 mm pavement + 50 mm UHPC + 12 mm deck plate; the longitudinal ribs are TN200 × 200 section steel with 500 mm lateral spacing, and the transverse ribs are TW100 × 200 section steel connected to the floorbeam below. The deck plate and UHPC are connected by Ø13 × 35 welded head studs with 150 mm spacing in longitudinal and transverse directions, and HRB400 reinforcement of Ø10 are arranged in the UHPC layer with 50mm spacing in both directions.

3.2 Comparison of bridge deck schemes

To compare the mechanical performance of OSD and SSD, software Ansys18.0 is used to establish the FE model of the main girder for both schemes (Fig. 6); the modeling and calculation methods are detailed in Subsection 4.1. The calculation results of two schemes are shown in Table 1. Overall, the stresses of two schemes are in similar ranges. Due to the addition of UHPC, the stress experienced by the SSD scheme in the deck plate is significantly reduced, from 40.1 MPa in the OSD scheme, to 23.2 MPa. On the other hand, due to the floorbeam of the SSD not extending and not being welded to the deck plate, the stress in the upper edge of floorbeam of the SSD scheme is larger than that of OSD scheme, while the deflection of the SSD is greater.

The two types of deck schemes are comprehensively compared and the results are shown in Table 2. Compared with OSD scheme, it can be seen that the steel usage, cost, and weld length of the SSD scheme are 18%, 18%, and 36% lower than those of the conventional OSD scheme, respectively, and the self-weight is comparable. Overall, the SSD has the advantages of good economy and easy processing, so it is a better bridge deck scheme than the OSD alternative.

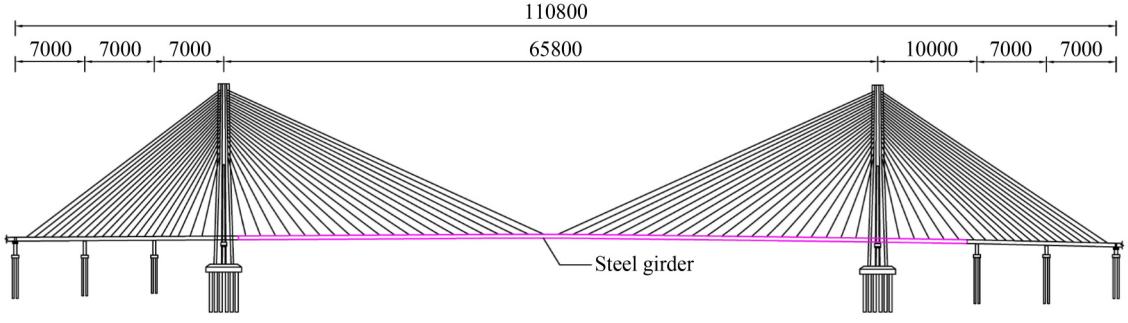

Fig. 5 Elevation layout of main bridge (unit: mm).

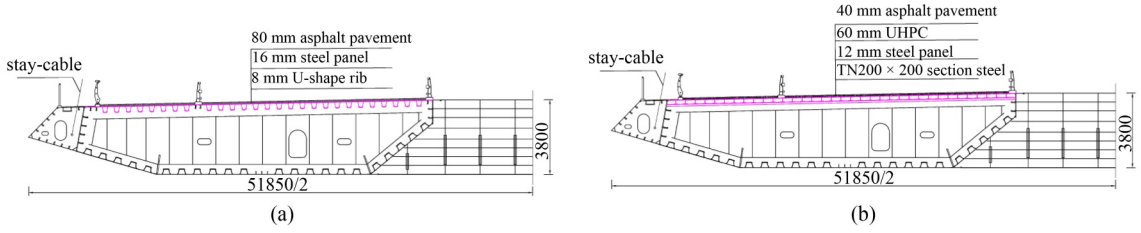

Fig. 6 Standard cross section of steel girder (unit: mm): (a) OSD scheme; (b) SSD scheme.

Table 1 Comparison of mechanical performance of OSD scheme and SSD scheme

Item	Type	OSD scheme	SSD scheme
Deck plate	max von mises stress (MPa)	40.1	23.2
Longitudinal rib	max von mises stress (MPa)	19.2	17.7
Floorbeam	max von mises stress (MPa)	45.5	61.7
Deck deflection	max deflection (mm)	0.95	1.69

Table 2 General comparison of OSD scheme and SSD scheme

Parameter	OSD scheme	SSD scheme
Self-weight (kg/m^2)	394.8	403.1
Steel usage (kg/m^2)	202.8	167.1
Cost of construction (RMB/m^2)	4443.3	3641.9
Weld length (m/m^2)	3.6	2.3
Manufacture	simple	complex

*Note: The index values in the table are as follows. Steel density: 7850 kg/m^3, UHPC density: 2800 kg/m^3, pavement density: 2400 kg/m^3. Welded steel price: 15000 RMB/t, hot-rolled section steel price: 10000 RMB/t, UHPC price: 1300 RMB /m^2, special asphalt pavement price in OSD: 1400 RMB/m^2, common pavement price in SSD: 200 RMB/m^2.

4 Study on static mechanical properties of hot-rolled section steel–ultra-high performance concrete composite deck with open ribs

4.1 Calculation and analysis of hot-rolled section steel–UHPC composite deck with open ribs

The stress acting on bridge decks includes the first system stress, the second system stress, and the third system stress. Based on the background project, the FE analysis software Midas civil 2019 is used to establish the whole bridge model, and the global stress of the bridge deck for the first system is calculated. Ansys18.0 is used to establish the solid-shell FE model of the main girder segment, and the local stress on the bridge deck for the second and the third systems is calculated. The FE model of the whole bridge and the main girder segment are shown in Fig. 7.

For the FE model of the main girder segment, a 15 m main girder segment in the longitudinal direction of the bridge is selected, which includes 4 floorbeams. To reduce the calculation scale, the cross-beam in the middle of the girder and the wind fairing in the side are not considered in the FE model. Since the main girder is a transverse symmetric separated double-box structure, only a 17.5 m wide single box girder is selected to build a segment model. In FE model of the main girder segment, 4-node shell element SHELL181 is used to simulate the steel structure, and 20-node solid element SOLID95 is used to simulate the UHPC. The material properties steel and reinforced UHPC in the FE model are considered as ideal linear elastic, and the properties of materials are shown in Table 3. In the FE model of the main girder segment, element COMBINE14 is used to simulate the head studs between deck plate and UHPC. The shear stiffness of the head studs in both longitudinal and transverse direction is 270 kN/mm. Compared to the connection strength of the head studs, the bonding

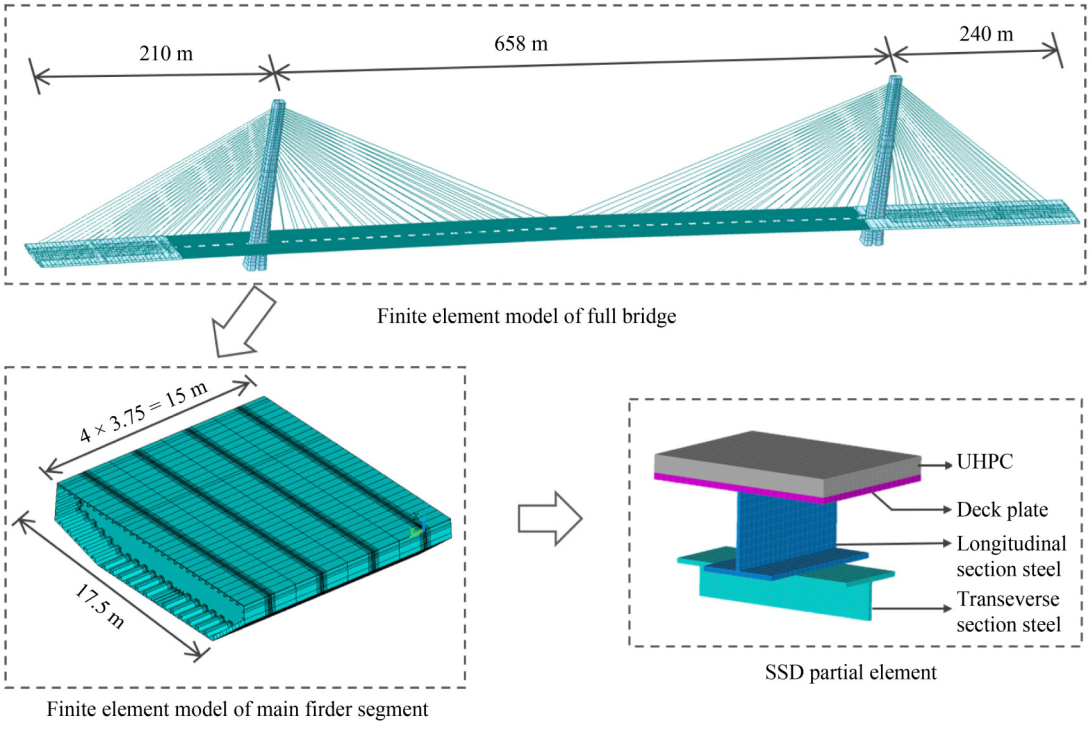

Fig. 7 FE calculation model of full-bridge and main girder segment.

Table 3 Properties of materials in FE model

Material	Elastic modulu (MPa)	Poisson's ratio	Density (kg/m^3)
Steel	2.06×10^5	0.3	7850
UHPC	4.97×10^4	0.2	2800

strength between UHPC and the steel deck plate is much weaker, so the bonding effect is ignored in the FE model, and the bonding effect is considered as a safety reserve. The connection welds between steel plates are simulated by means of nodal coupling. Element CONTA173 and TARGE170 are used for the contact surfaces of flange plates of longitudinal and transverse section steel, respectively, to simulate the force transfer effects of compression contact and tensile separating of contact surfaces.

The boundary conditions of the main girder segment model are as follows: the longitudinal, transversal and vertical translational degrees of freedom are constrained at the longitudinal end of the main girder. The vertical translational freedom of the anchorage cable joints of the main girder are constrained. Load includes the self-weight of the bridge deck and vehicle load. The vehicle load adopts the provisions of China steel bridge specification [45]. The total weight of vehicle load is 550 kN, which is set according to the most unfavorable conditions of the three lanes in one direction.

The stress calculation results of the SSD are summarized in Table 4, where the longitudinal stress is the sum of the first, the second and the third system stresses, while the transverse stress is the sum of the second and the third system stresses, which are obtained by FE model of the main girder segment. The max stresses calculated by the whole bridge FE model and main girder segment FE model may not occur exactly at the same point, but in the same small area. Considering the most unfavorable situation for safety [26], the total stresses are the sum of the max stresses calculated by the two FE models as shown in Table 4. The maximum stress of the deck plate is 134.5 MPa and the maximum stress of the longitudinal section steel is 135.7 MPa; these are both less than the design value 270 MPa, based on Chinese steel bridge specification [45]. The maximum compressive stress acting on the UHPC is 26.6 MPa, which is much less than the compressive strength 151.4 MPa (Table 5). The maximum tensile stress of the UHPC is 5.9 MPa. According to Ref. [31] the transverse tensile strength of the bridge deck UHPC (steel + UHPC) is more than 17.2 MPa, which is 2.9 times the stress of the background bridge. In conclusion, the peaked stresses in the SSD components are less than the corresponding allowable strengths, so can meet the stress requirements of the background bridge.

4.2 Static test of negative bending moment strip of hot-rolled section steel–ultra-high performance concrete composite deck with open ribs

As we all know, the UHPC layer of the SSD is in a state of tension under the negative bending moment. The maximum tensile stress of UHPC (Table 4) in the longitudinal direction is 10.1 MPa. The cracking resistance of UHPC affects the durability of the bridge deck structure in service. Therefore, a static test of negative bending moment strip of the SSD is carried out to study the mechanical properties of UHPC.

4.2.1 Model loading and testing

Referring to the SSD structure of the background project bridge, a single longitudinal rib strip is selected. The dimensions of the strip specimen are 2800 mm × 500 mm × 700 mm (length × width × depth), as shown in Fig. 8. In the longitudinal direction, the specimen includes a simply-supported part and a cantilever end, and the lengths of the simply-supported and cantilever parts are 1000 and 1300 mm, respectively. While in the depth direction, the specimen consists of an SSD deck and a diaphragm and supporting structures.

The materials of the strip specimen are identical to those of the background bridge. For steel, the grade of the steel plate and section steel is Q345. While for the UHPC layer, the length and diameter of the steel fibers are 13 and 0.2 mm, respectively, and the volume fraction is 2%. The basic properties of the UHPC are presented in Table 5.

To generate a negative bending moment at the front fulcrum, the strip specimen is loaded at the cantilever end, as shown in Fig. 9. Two floorbeam bases are placed on the steel pier. At the top surface of the back fulcrum,

Table 4 Summary of stress calculation results of the SSD

Specimen	Stress direction	FE model of full bridge	FE model of main girder	Sum
Deck plate	longitudinal direction	[–118.4,35.9]	[–16.1,15.6]	[–134.5,51.5]
	transverse direction	–	[–18.3,23.2]	[–18.3,23.2]
Longitudinal section steel	longitudinal direction	[–114.2,35.7]	[–21.5,17.7]	[–135.7,53.4]
UHPC	longitudinal direction	[–20.7,2.3]	[–5.9,7.8]	[–26.6,10.1]
	transverse direction	–	[–9.8,5.9]	[–9.8,5.9]

*Note: Stress unit is MPa, tensile stress is "+", compressive stress is "–".

Table 5 Basic material properties of UHPC

Compressive strength (MPa)	Flexural strength (MPa)	Axial tensile strength (MPa)	Elastic modulus (GPa)
151.4	21.6	8.0	49.7

the ground anchored beam is used to provide pressure to balance the loading force. The PMZ4.0 hydraulic equipment is used for loading, and the distance from the loading position to the front fulcrum of the floorbeam is 1.0 m. The load is increased by 2.5 kN at each stage starting from 0, until the specimen is damaged.

The negative bending moment at the front fulcrum is the largest, so the tensile stress on the top surface of the UHPC layer reaches the maximum. The digital image correlation (DIC) technique [34] is used to measure the crack width and strain of UHPC at each loading stage. The measurement region of DIC is 600 mm × 500 mm (length × width), which is located on the top surface of the UHPC at the front fulcrum, as shown in Fig. 9(a). Matte white lacquer is painted on the UHPC surface in the measurement region, and then black dots with a diameter of about 0.8 mm are evenly and densely sprayed on the white paint surface. Two high-definition CCD cameras are set up above the specimen, and the black dots images on the surface of UHPC layer are captured by the CCD cameras after each stage of loading.

4.2.2 Analysis of test results

Post-processing software VIC-3D is used for DIC analysis, and the surface crack distribution of UHPC under maximum load is obtained in measurement region of DIC, as shown in Fig. 10. According to the occurrence sequence of cracks, a total of 20 cracks are numbered from C1 to C20. The data in the bracket of Fig. 10 is the maximum crack width (unit: mm) for each numbered crack. As the load increases, more and more cracks appear and extend to both sides. Among all the cracks, the width of C1, C5, and C6 are the largest, which are concentrated on the top surface of the front fulcrum of the floorbeam.

The load–crack width curves of the main cracks is shown in Fig. 11. When the load is 45.0 kN, the first crack C1 appear and the crack width is 0.02 mm. When the load increases to 90.0 kN, the crack width of C1 reaches 0.05 mm. At the maximum load of 187.5 kN, the crack width reaches 0.13 mm. Crack C1 is the first crack

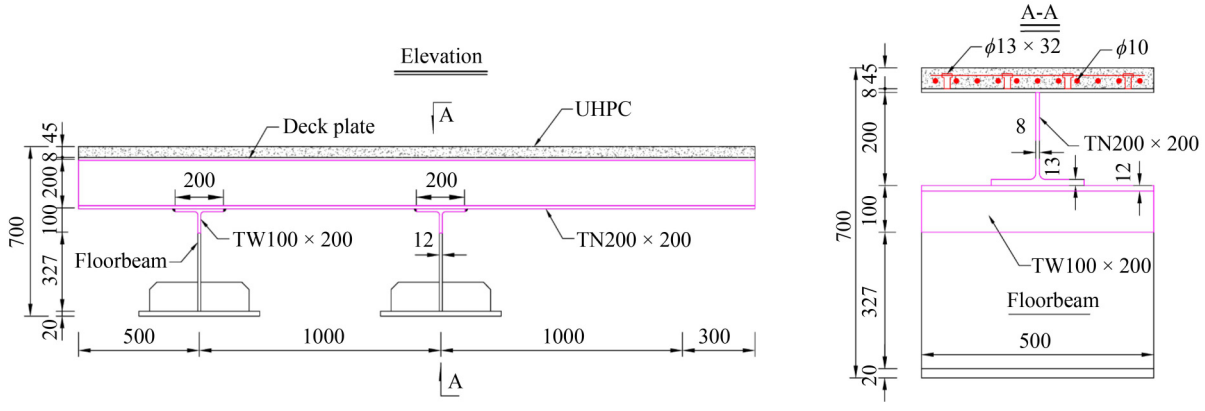

Fig. 8 Details of strip specimen (unit: mm).

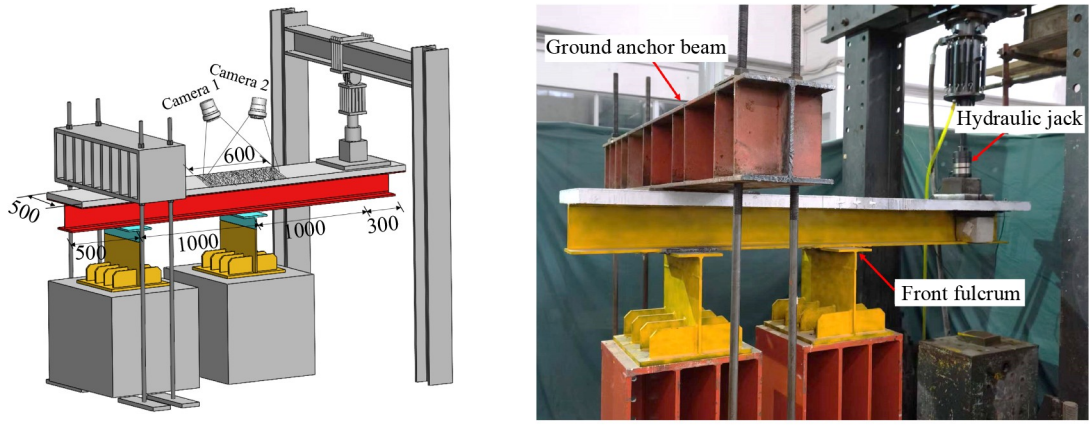

(a) (b)

Fig. 9 Static test of strip specimen (unit: mm): (a) loading and testing setup; (b) site loading of strip specimen.

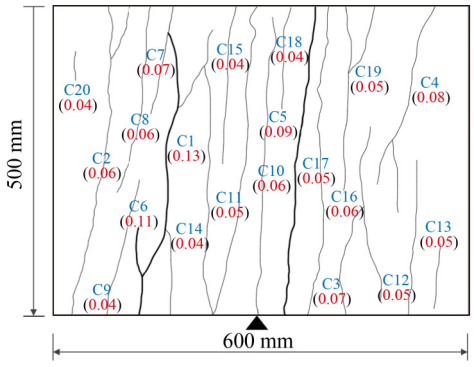

Fig. 10 UHPC surface cracks distribution (unit: mm).

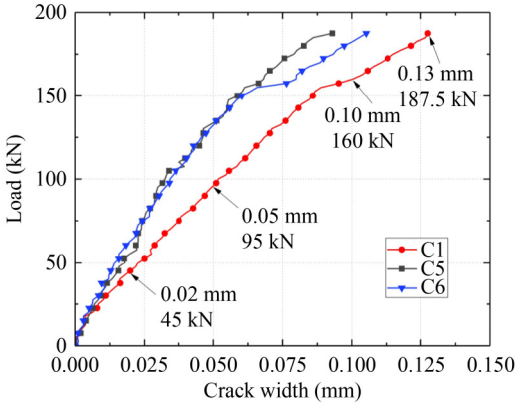

Fig. 11 Load–crack width curves.

to appear and the width of C1 is the largest at all level, so C1 is defined as the dominant crack. The widths of all cracks increase linearly with the increase of load, indicating that the steel fibers in the UHPC play an excellent role in bridging the material. After the initial cracking of UHPC, the stress is transferred to the surrounding uncracked UHPC. UHPC shows good tensile toughness.

After loading to the maximum load of 187.5 kN, a large angle appears between the web and the upper flange plate of the front floorbeam, and the bearing capacity of the specimen drops rapidly, so the test is stopped. There are no cracks in the fillet welds between the longitudinal and transverse ribs, indicating that the connection between the longitudinal and transverse ribs have reliable connection strength. The failure mode of the specimen is the yield instability of the steel structure at the floorbeam. Before that, no strength failure occurs in the longitudinal ribs, UHPC layers, or the connection welds of the longitudinal and transverse ribs, indicating that the SSD structure has good bearing capacity.

When the surface crack width of UHPC is no more than 0.05 mm, the durability of UHPC is not affected [32]. Therefore, the maximum crack width limit of UHPC is 0.05 mm in this work, to ensure the durability of the bridge deck structure. The corresponding load is 95.0 kN at 0.05 mm crack width for the main crack C1 (Fig. 11). And the corresponding nominal cracking stress of the UHPC layer of SSD is 18.1 MPa, which is calculated by the elastic method. The calculated stress is 1.8 times the maximum tensile stress of 10.1 MPa (Table 4) of the background bridge, which can meet the requirements of the background bridge, and has a large safety reserve.

4.2.3 Theoretical calculation analysis

To predict the bending behavior of the SSD, a theoretical calculation method model is proposed. The following assumptions are applied: 1) the cross-section of SSD under negative bending moment remains flat; 2) considering the tensile strength of UHPC after cracking, the post-crack strength of UHPC is taken as axial tensile strength f_{ct}; 3) before yielding, section steel and reinforcement are ideal elastic materials, and the stress is proportional to the strain. The calculation model of SSD is shown in Fig. 12.

According to the balance of the axial force and bending moment, the Eqs. (1) and (2) can be obtained:

$$N_c + N_r + N_d + N_b - N_l = 0, \tag{1}$$

$$M_c + M_r + M_d + M_b - M_l = 0, \tag{2}$$

where N_c, N_r, N_d, and N_b are the internal axial forces

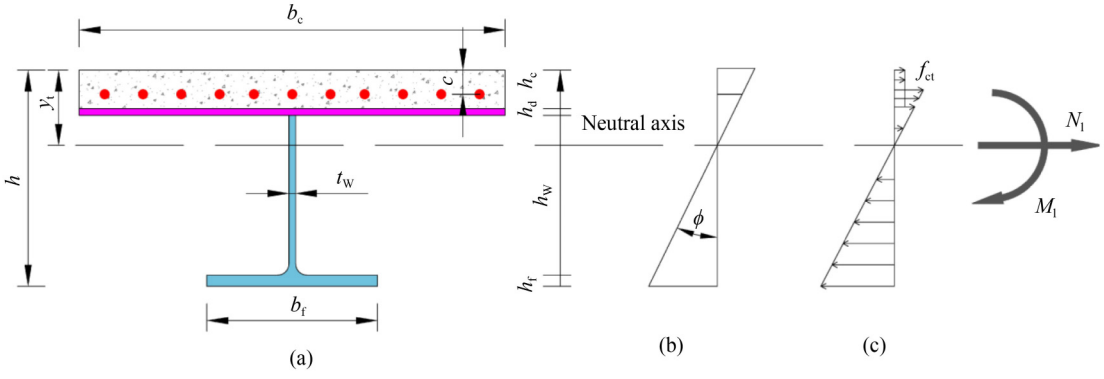

Fig. 12 Calculation model of SSD: (a) cross-section; (b) strain distribution; (c) stress distribution.

carried by UHPC, reinforcement, deck plate and longitudinal rib, respectively, and N_l is external axial force. M_c, M_r, M_d, and M_b are the internal bending moments carried by UHPC, reinforcement, deck plate and longitudinal rib, respectively, and M_l is the bending moment generated by external load.

The internal axial forces and bending moments of each component of SSD can be calculated by integrating the stresses in the cross-section based on Fig. 12.

$$N_c = f_{ct} b_c h_c, \tag{3}$$

$$N_r = E_r A_r \phi (y_t - c), \tag{4}$$

$$N_d = E_s b_c h_d \phi (y_t - h_c - h_d/2), \tag{5}$$

$$N_b = E_s t_w \phi \left[(y_t - h_c - h_d)^2 - (h - y_t - h_f)^2\right]/2 - E_s b_f h_f \phi (h - y_t - h_f/2), \tag{6}$$

$$M_c = N_c (y_t - h_c/2), \tag{7}$$

$$M_r = N_r (y_t - c), \tag{8}$$

$$M_d = N_d (y_t - h_c - h_d/2), \tag{9}$$

$$M_b = E_s t_w \phi \left[(y_t - h_c - h_d)^3 - (h - y_t - h_f)^3\right]/3 - E_s b_f h_f \phi (h - y_t - h_f/2)^2, \tag{10}$$

where b_c is the width of deck plate, t_w and b_f are the thickness of longitudinal rib web and width of longitudinal rib flange plate, respectively; h_c and h_w are the heights of UHPC and longitudinal rib web, respectively; h_d and h_f are the thickness of steel deck plate and longitudinal rib flange plate, respectively; y_t is the distance from the neutral axis to the top surface of UHPC; h is the total height of SSD; A_r is the reinforcement area; c is the distance from the center of reinforcement to the top surface of UHPC; f_{ct} is axial tensile strength of UHPC. E_r is elastic modulus of reinforcement; E_s is the elastic modulus of steel; ϕ is the bending curvature of the cross-section of SSD.

Substituting Eqs. (3)–(6) into the axial force balance Eq. (1) and substituting Eqs. (7)–(10) into the bending moment balance Eq. (2), then Eqs. (1) and (2) can be solved simultaneously to obtain the two unknowns: the bending curvature of the cross-section ϕ and the height of the neutral axis y_t. Finally, according to Eq. (11), the strain at any height of the cross-section can be obtained, and the stress level of each component can be obtained from the material properties.

$$\varepsilon_i = \phi y_i, \tag{11}$$

where ε_i is the strain value; y_i is the distance from the calculated position to the neutral axis.

The load–strain curve of test and theoretical calculation is shown in Fig. 13. The average strains (S1 to S9) occurring on the top surface of UHPC at the front fulcrum are obtained by DIC test, and the test resluts are compared with that of the theoretical formula. The strain of UHPC increases linearly with the increase of load, and the whole reinforced UHPC is in an excellent elastic stress range. The overall trend of load–strain curve calculated by experiment and theoretical formula is in good agreement. The maximum strain obtained by test and calculation under maximum load is 1248 × 10^{-6} and 1209 × 10^{-6}, respectively, with a difference of about 3%, which indicates that the theoretical formula proposed in this paper can relative accurately calculate the strain of SSD.

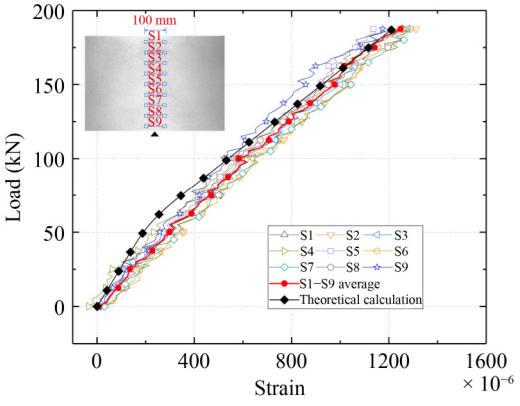

Fig. 13 Load–strain curves of test and theoretical calculation.

5 Study on fatigue performance of hot-rolled section steel–ultra-high performance concrete composite deck with open ribs

5.1 Fatigue-prone detail and strength classification

To study the fatigue performance of OSD, and to compare with conventional OSDs, calculation and evaluation of three different deck structures are carried out. Figure 14(a) shows the conventional OSD with U-shape rib, Fig. 14(c) shows the SSD proposed in this paper. Figure 14(b) shows the conventional steel–UHPC composite deck with T-shaped rib (CSSD). The difference between of SSD and CSSD is that the longitudinal ribs and floorbeam of CSSD are connected by conventional cutouts through welding.

The fatigue failure of steel structures can be divided into two types: the first type is fatigue caused by welding, and the second type is fatigue caused by stress concentration in non-welded positions due to structural geometry. According to previous research and applications [27,28],

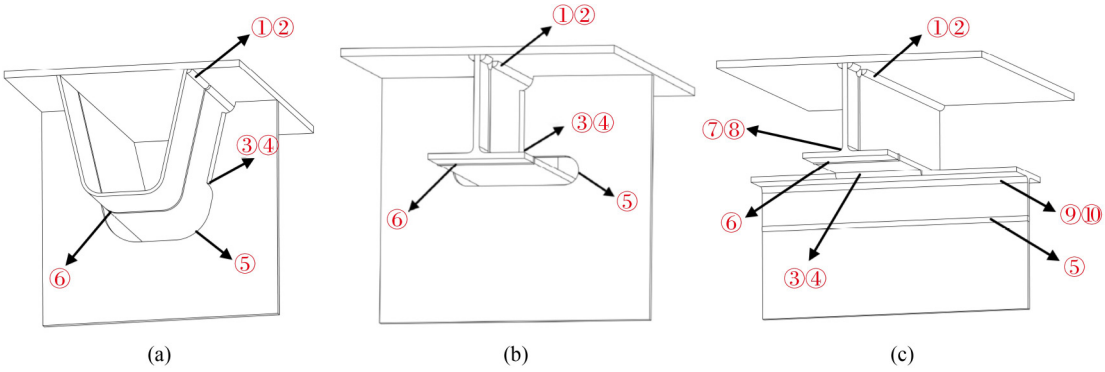

Fig. 14 Classification of fatigue-prone location details of different deck schemes: (a) OSD; (b) CSSD; (c) SSD.

OSD and CSSD include six fatigue-prone locations that are prone to cracking (Figs. 14(a) and 14(b)): fatigue-prone locations ① and ② are cracks at the deck plate and longitudinal rib of RD joint, respectively; fatigue-prone locations ③ and ④ are cracks at longitudinal rib web and floorbeam of RF joint, respectively; fatigue-prone location ⑤ indicates cracks at the cutout edge of the floorbeam; fatigue-prone location ⑥ indicates cracks at the connection welds of the longitudinal rib.

Currently there is no engineering application or research reference in SSD. Therefore, all possible positions for fatigue cracking are defined as fatigue-prone location details in the preliminary study, as shown in Fig. 14(c). Fatigue-prone detail locations ①–⑥ show locations of the first type of fatigue: fatigue-prone detail locations ① and ② show cracks at the deck plate and longitudinal rib of RD joint, respectively; fatigue-prone detail locations ③ and ④ show cracks at the longitudinal and transverse rib flange plates of the longitudinal and transverse rib connection welds, respectively; fatigue-prone detail location ⑤ indicates cracks at the butt weld between transverse rib web and floorbeam; fatigue-prone detail location ⑥ indicates cracks at the connection welds of the longitudinal rib. Fatigue-prone detail locations ⑦–⑩ show locations of the second type of fatigue: fatigue-prone detail locations ⑦ and ⑧ are cracks at the joint of longitudinal section steel web and flange plate, respectively; fatigue-prone detail locations ⑨ and ⑩ are locations of cracks at the joint of transverse section steel web and flange plate, respectively.

The S–N curve method based on Miner's criterion is mainly used for fatigue evaluation of steel structures, and the methods commonly include the nominal stress method and the hot spot stress method. For the fatigue stress at welding position of complex structures, it is appropriate to use the hot spot stress method recommended by International Institute of Welding (IIW) [46]. The stresses at two points at distances of 0.5 and 1.5 t (t represents the thickness of the steel plate) from the weld toe are extracted and linearly extrapolated to obtain the hot spot stresses. For the fatigue stress in non-welded position, it is appropriate to use the nominal stress method, which is widely used in current steel bridge codes [45,47]. The fatigue-prone detail classification and fatigue strength of three different bridge deck types are shown in Table 6, in which the fatigue-prone detail category corresponds to 2 million loading cycles, and the constant amplitude fatigue limit corresponds to 5 million loading cycles.

5.2 Fatigue calculation and evaluation

According to the three bridge deck schemes (see Fig. 14), three different FE models of the main girder segments are established for fatigue calculation and analysis, respectively. Except for the differences in the bridge deck structures, the model dimensions, material elements and constrained boundary conditions of the FE models are consistent with Subsection 4.1. According to the Chinese steel bridge specification [45], a single fatigue vehicle is

Table 6 The fatigue-prone detail classification and fatigue strength of different deck types

Detail location number	OSD and CSSD		SSD	
	Fatigue-prone detail category (MPa)	Constant amplitude fatigue limit (MPa)	Fatigue-prone detail category (MPa)	Constant amplitude fatigue limit (MPa)
①, ②	90	58	90	58
③, ④	90	58	90	58
⑤	125*	80*	90	58
⑥	90	58	90	58
⑦–⑩	–	–	160*	103*

*Note: The nominal stress method is used, while the hot spot stress method is used if there is no special mark.

used for fatigue loading, with a total weight of 480 kN and a single axle weight of 120 kN. At different transverse wheel positions, the fatigue vehicle is loaded from one side of the main girder to the other end by longitudinal movement to obtain the fatigue-prone detail stress history, and finally the maximum stress amplitude of each fatigue-prone detail is obtained by the rain-flow method.

The fatigue stress amplitude calculated by the FE model is shown in Table 7. Conventional OSD with U-shape rib have much higher fatigue stresses at RD joint and RF joint; stresses at fatigue-prone details ① to ⑤ are larger than constant amplitude fatigue limit, therefore the fatigue resistance of OSD is poor. Compared with OSD, due to the addition of UHPC as the structural layer, CSSD has better fatigue resistance, stresses at fatigue-prone details ① and ②, at RD joints, are reduced by 83% and 71%, respectively, stresses at fatigue-prone details ③ and ④ stresses at RF joint have relatively small stress reduction, with stress decreases of 53% and 55%, respectively, but the stress at fatigue-prone detail ⑤ at the cutout edge is still high, with a high risk of cracking.

Compared with in the CSSD case, stresses at fatigue detail locations ① and ②, at RD joint of SSD, are at the same low level. Furthermore, the SSD optimizes the longitudinal and transverse rib connection structure, and eliminating the floorbeam cutouts, stresses at fatigue details ③ to ⑤, at RF joints, are significantly reduced, the maximum fatigue stress at RF joint does not exceed 40.9 MPa. Stresses at fatigue detail locations ⑦ to ⑩ have relatively large values, with a maximum of 96.4 MPa. If welded steel plates are used instead of T-shape section steel, the fatigue strength at detail locations ⑦–⑩ is decreased from 160 to 80 MPa, indicating a high risk of fatigue cracking. Therefore, the use of hot-rolled section steel in SSD is very essential. In summary, all the fatigue detail stresses of SSD are below the constant amplitude fatigue limit, so SSD has the best fatigue resistance.

Table 7 Fatigue stress amplitude calculation results of different deck types

Fatigue position	Detail number	Fatigue stress amplitude (MPa)		
		OSD	CSSD	SSD
RD joint	①	130.0	22.1	29.1
	②	102.1	29.4	40.3
RF joint	③	120.3	56.8	40.9
	④	138.4	61.6	24.4
	⑤	110.5	112.2	26.0
Longitudinal rib connection	⑥	41.3	31.8	29.6
Section steel base material	⑦	–	–	96.4
	⑧	–	–	49.0
	⑨	–	–	47.0
	⑩	–	–	58.8

In summary of the above calculation and analysis, the SSD is expected to completely solve the fatigue problem of bridge steel deck due to four benefits. 1) For the RD joint (details ① and ②), using UHPC as the structural layer increases the local stiffness and reduces the fatigue stress of the deck plate. 2) For the RF joint (details ③ and ④), the connection between the ribs and the floorbeam are overlapped from top to bottom to replace the conventional opening, so that the connection structure is greatly simplified, thereby reducing the stress concentration effect of RD joint. 3) For the necessary connection welds (details ⑤ and ⑥), the welds are placed in the low stress zone to avoid high fatigue stress. 4) For the web and flange plate joint of T-shape section steel (details ⑦–⑩) the stress concentration effect cannot be avoided, but the use of one-piece hot-rolled section steel instead of welded steel plate significantly improves the fatigue limits, thereby greatly improving the fatigue resistance of the bridge deck.

5.3 Key design parameters of hot-rolled section steel–ultra-high performance concrete composite deck with open ribs on fatigue performance

To study the influence of key design parameters of SSD on fatigue performance, four key design parameters including thickness of UHPC and steel deck, height and spacing of longitudinal rib, are selected as the variables. And to eliminate the mutual influence of multi-variable parameters, a single variable is used for FE calculation and analysis. The value of one parameter is changed each time, and the other parameters remain unchanged from the background bridge. For SSD of the background bridge, the thickness of UHPC is 50 mm, the thickness of the deck plate is 12 mm, and the height and spacing of the longitudinal ribs are 200 and 500 mm. The selected values of design parameters (Table 8) are within the reasonable range, based on the real bridge application.

Table 8 The values of key design parameters

Design parameter	Initial value (mm)	Value range (mm)
Thickness of UHPC	50	0, 30, 40, 50, 60, 70, 80
Thickness of steel deck	12	8, 10, 12, 14, 16, 18
Height of longitudinal rib	200	150, 200, 250, 300, 350, 400
Spacing of longitudinal rib	500	300, 400, 500, 600, 700, 800

According to Table 8, 21 FE models of the main girder segment including 4 groups of design parameters are established. The calculation methods are the same as those in Subsection 5.2. Under the loading of fatigue vehicle, the time-history curves of fatigue stress at each fatigue-prone detail position are extracted from the FE

models. The fatigue stress amplitude of each fatigue-prone detail of SSD under different design parameters is shown in Fig. 15.

When the thickness of UHPC is increased from 0 to 40 mm, the stress decrease is the most obvious at fatigue-prone details ① and ② at RD joint, with reductions of 76% and 58%, respectively, and stresses at other fatigue-prone detail locations are reduced by 14%–33%. When UHPC thickness reaches a value of 60 mm, the stress amplitude at each fatigue-prone location has been significantly reduced, but continuing to increase the UHPC thickness has limited effect on the reduction of fatigue stress. If UHPC thickness is less than 40 mm, it is difficult to meet the minimum thickness required for the reinforcement arrangement and protective layer requirements. If the UHPC thickness is more than 60 mm, the material consumption and the dead load increased, and the effect on fatigue performance improvement is relatively small. Considering the structural requirements and fatigue performance, the thickness of UHPC is recommended to be between 40 and 60 mm, which is the thickness range used in most real bridge projects.

When the thickness of the deck plate increases from 8 to 18 mm, the stress of fatigue-prone detail locations ① at the deck plate decreases from 35.1 to 24.1 MPa with a reduction of 31%, while the stresses at other fatigue-prone detail locations remain basically unchanged with a reduction no more than 3%. After adopting UHPC, the stress of fatigue-prone detail ① is significantly reduced; increasing the thickness of the deck plate has no obvious effect on improving the fatigue resistance of SSD. Compared with the 16 mm or thicker deck plate commonly used for conventional OSD, the thickness of the deck plate of SSD can be reduced appropriately to reduce steel consumption and save cost.

When the height of longitudinal rib increases from 150 to 400 mm, the stresses of fatigue-prone detail ② in the longitudinal rib web and fatigue-prone detail ③ in the longitudinal rib flange decrease by 53% and 62%, respectively, while the stresses of other fatigue-prone detail locations remain basically unchanged. With the increase of the height of the longitudinal ribs, the flexural stiffness of the longitudinal ribs is increased, so the flexural stress of the longitudinal ribs under the action of vehicular load is reduced. The height of open ribs is mostly between 200 and 300 mm in real projects. Thus, the height of the longitudinal ribs of SSD should be set by comprehensively considering the height of the main beam and the span of the floorbeams, in line with the stress requirements of the whole bridge structure.

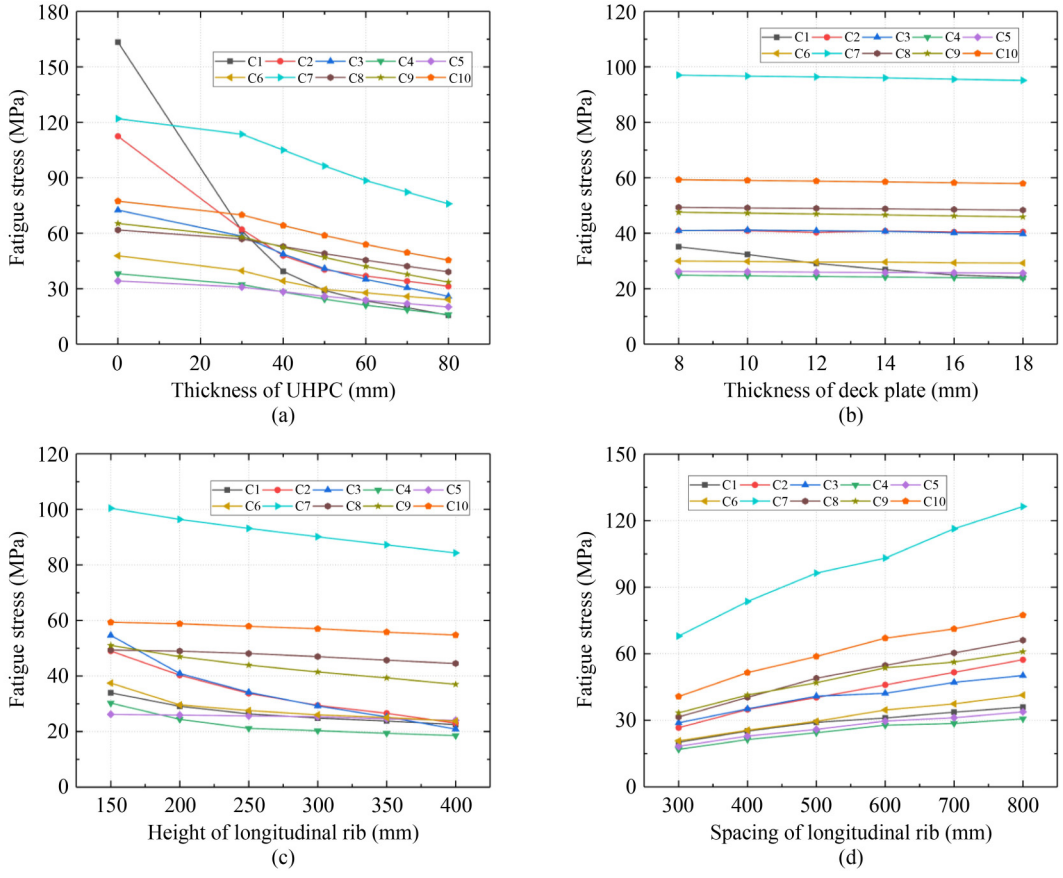

Fig. 15 Fatigue stress amplitude under different design parameters: (a) thickness of UHPC; (b) thickness of deck plate; (c) height of longitudinal rib; (d) spacing of longitudinal rib.

When the spacing of longitudinal ribs increased from 300 to 800 mm, the stresses of all fatigue-prone details increased by the same amplitudes, indicating that the spacing of longitudinal ribs has a great influence on the fatigue performance of the SSD. As the spacing of longitudinal ribs decreases, more longitudinal ribs carry the load under a single wheel load, and the fatigue performance of each fatigue-prone detail can be improved. The spacing of open ribs in OSD is mostly between 300 and 400 mm. As UHPC greatly increases the transverse stiffness of the deck plate, the spacing of longitudinal ribs in SSD can be appropriately increased. Meanwhile, the transverse width of a single wheel is 600 mm according to the Chinese steel bridge specification [47], so in order to prevent the wheels directly acting on the deck plate without longitudinal stiffeners and causing punching damage to the UHPC, the spacing of longitudinal ribs should not exceed the width of a single wheel. Therefore, it is recommended that the transverse spacing of longitudinal ribs should be between 400 and 600 mm.

5.4 Fatigue test of negative moment strip of hot-rolled section steel–ultra-high performance concrete composite deck with open ribs

Due to the fact that longitudinal and transverse ribs in SSD are connected by a new type of structure, the welded connection (fatigue-prone details ③ and ④) between the longitudinal and transverse ribs is determined as the key concern. The connecting welds are at the bottom of the longitudinal ribs, which is in the negative bending moment area. So the fatigue stress of the connecting welds is mainly compressive. Based on this, a fatigue test is carried out for another SSD strip specimen to investigate the fatigue behavior of the connection welds of the longitudinal and transverse ribs.

5.4.1 Model loading and testing

A single strip of SSD is selected for the fatigue test. The specimen structure and loading device are consistent with the static test in Subsection 4.2, but the load is changed from static loading to dynamic loading. The fatigue loading is divided into three stages. Stage I: fatigue load range is 6–23 kN, for 2 million times of loading cycles; Stage II: load range is 6–40 kN, for 2 million times of loading cycles; Stage III: fatigue load range is 6–57 kN, loading to fatigue damage. In the process of fatigue test, the fatigue loading machine is shut down for static load testing every 250000 loading cycles, and the static load is gradually loaded from 0 to the upper peak of the fatigue load. The strain data of fatigue-prone details is collected during the static load process.

5.4.2 Analysis of test results

With the accumulation of fatigue loading cycles, the fatigue stress amplitude at the connecting welds is shown in Fig. 16. The hot spot stress of the connecting welds is about 51.4 MPa in stage I, and no fatigue damage in the structure at this stage. Stage II doubles the load amplitude, and the hot spot stress is simultaneously doubled to about 101.9 MPa, indicating that the structure is in a good elastic state. In stage III, the load amplitude is trebled (relative to stage I), and the hot spot stress increases from 151.1 MPa in the previous stage to 178.6 MPa after a total of 4.25 million loading cycles. The stress amplitude increases by 18%, indicating that the fillet welds begin to crack at this stage. When the loading cycles reach 4.62 million times, the fatigue cracks in the throat of connecting welds are completely penetrated, indicating the complete fatigue damage of the structure.

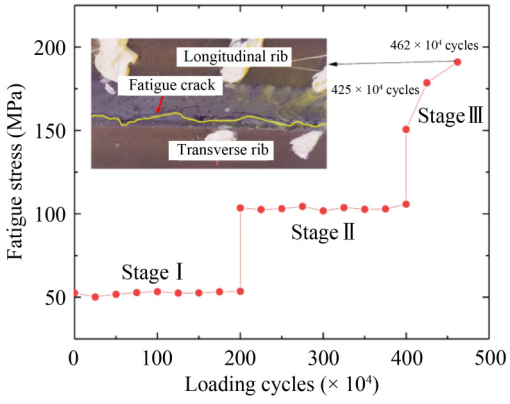

Fig. 16 Fatigue stress amplitude of connecting weld under different loading cycles.

Based on the Miner criterion for linear accumulation of damage, 4.25 million variable amplitude fatigue loading cycles can be equivalent to 47.5 million loading cycles for the design fatigue stress range 40.9 MPa (Table 7). According to the S–N curve recommended by IIW [45], if the fatigue-prone detail location is not damaged after more than 10 million cycles of loading, it can be considered to have infinite fatigue life. Therefore, the loading cycles of 47.5 million times far exceeds the demanded cycles of the background bridge. In summary, the fatigue behavior of the fillet weld between the longitudinal and transverse ribs of SSD meets the design requirements, and can be regarded as the non-cracking fatigue-prone details in the real bridge.

6 Conclusions

In this paper, a new steel–UHPC composite deck, the SSD is proposed. Based on a long-span cable-stayed bridge, a detailed FE analysis is conducted for the SSD,

and a static test and a fatigue test are performed to verify the anti-cracking behavior and the fatigue behavior of the new bridge deck structure. Based on the current investigations, the following conclusions can be drawn.

1) Compared with the conventional OSDs, the SSDs use low-cost hot-rolled steel instead of welded steel plates, and the longitudinal ribs and the diaphragms are stacked up and down, which is more simple to fabricate. Thus, the cost of the new bridge deck structure is reduced by 18% and the weld length can be reduced up to 36%.

2) The static experimental test is conducted for the SSD strip specimen, and the results show that under the allowable maximum crack state (i.e., 0.05 mm), the nominal cracking stress of the UHPC layer in the specimen is 18.1 MPa, which is 1.8 times the maximum tensile stress of the background bridge. A theoretical calculation method based on the proposed method could yield satisfactory accuracy relative to the test results.

3) The FE analysis results show that the maximum stress range for all the fatigue-prone detail locations are below the corresponding constant amplitude fatigue limit, implying that theoretically the fatigue performance of the SSD could meet the design requirements. Among the key design parameters of SSD, the thickness of UHPC and the transverse spacing of the longitudinal ribs have greater impacts on fatigue performance.

4) A fatigue test is conducted to verify the fatigue performance of the key fillet welds of the SSD. The specimen fails after 47.52 million cycles of loading within the design fatigue stress range, which significantly exceeded the design fatigue life. This implies that the welded connection between the longitudinal and transverse ribs can be basically regarded as non-cracking fatigue-prone detail.

5) In summary, SSD is an innovative bridge deck structure with excellent mechanical performance and potential applications. Its ultimate capacity, stability and design method are the subjects of the following research.

Acknowledgements The authors gratefully thank the National Natural Science Foundation of China (Grant Nos. 52038003 and 51778223) and Technology R&D Plan of China Construction Fifth Engineering Division Co., Ltd. (No. CSCES5b-2022-12) for their financial support.

Competing interests The authors declare that they have no competing interests.

References

1. AISC. Design Manual for Orthotropic Steel Plate Deck Bridges. New York: American Institute of Steel Construction, 1963
2. Wolchuk R. Lessons from weld cracks in orthotropic decks on three European bridges. Journal of Structural Engineering, 1990, 116(1): 75−84
3. Tsakopoulos P A, Fisher J W. Full-scale fatigue tests of steel orthotropic Decks for the Williamsburg bridge. Journal of Bridge Engineering, 2003, 8(5): 323−333
4. Cao B Y, Ding Y L, Song Y S, Zhong W. Fatigue life evaluation for deck-rib welding details of orthotropic steel deck integrating mean stress effects. Journal of Bridge Engineering, 2019, 24(2): 04018114
5. Xiao Z G, Yamada K, Inoue J, Yamaguchi K. Fatigue cracks in longitudinal ribs of steel orthotropic deck. International Journal of Fatigue, 2006, 28(4): 409−416
6. Wu W, Kolstein H, Veljkovic M. Fatigue resistance of rib-to-deck welded joint in OSDs, analyzed by fracture mechanics. Journal of Constructional Steel Research, 2019, 162: 105700
7. Li J, Zhang Q H, Bao Y, Zhu J, Chen L, Bu Y. An equivalent structural stress-based fatigue evaluation framework for rib-to-deck welded joints in orthotropic steel deck. Engineering Structures, 2019, 196: 109304
8. Liu R, Liu Y Q, Ji B, Wang M, Tian Y. Hot spot stress analysis on rib–deck welded joint in orthotropic steel decks. Journal of Constructional Steel Research, 2014, 97(6): 1−9
9. Fu Z Q, Ji B, Zhang C, Wang Q. Fatigue performance of roof and U-rib weld of orthotropic steel bridge deck with different penetration rates. Journal of Bridge Engineering, 2017, 22(6): 04017016
10. Wang K, Jie Z, Liang S D, Zhuge P. Fatigue assessment of U-rib full penetration welded joints based on local methods. Journal of Constructional Steel Research, 2023, 200: 107684
11. Fang Z, Ding Y, Wei X, Li A, Geng F. Fatigue failure and optimization of double-sided weld in orthotropic steel bridge decks. Engineering Failure Analysis, 2020, 116: 104750
12. Heng J, Zheng K, Gou C, Zhang Y, Bao Y. Fatigue performance of rib-to-deck joints in orthotropic steel decks with thickened edge U-ribs. Journal of Bridge Engineering, 2017, 22(9): 04017059
13. Luo P J, Zhang Q H, Bao Y Z, Bu Y. Fatigue performance of welded joint between thickened-edge U-rib and deck in orthotropic steel deck. Engineering Structures, 2019, 181: 699−710
14. Wang B, Lu P, Shao Y. Research on rib-to-diaphragm welded connection by means of hot spot stress approach. Steel and Composite Structures, 2015, 18(1): 135−148
15. Castiglioni C A, Fisher J W, Yen B T. Evaluation of fatigue cracking at cross diaphragms of a multigirder steel bridge. Journal of Constructional Steel Research, 1988, 9(2): 95−110
16. Cui C, Hu J D, Zhang X, Zeng J, Li J, Zhang Q. Fatigue test and failure mechanism of new rib-to-floorbeam welded joints in OSDs. Journal of Constructional Steel Research, 2023, 203: 107835
17. Connor R J. Influence of cutout geometry on stresses at welded rib-to-diaphragm connections in steel orthotropic bridge decks. Transportation Research Record: Journal of the Transportation Research Board, 2004, 1892(1): 78−87
18. Zhu Z W, Xiang Z, Li J, Huang Y, Ruan S. Fatigue behavior of orthotropic bridge decks with two types of cutout geometry based on field monitoring and FEM analysis. Engineering Structures, 2020, 209: 109926
19. Di J, Wang J, Zhou X, Peng X, Qin F. Fatigue behavior of rib-to-floor beam junctions with separate inner stiffeners in orthotropic steel bridge decks. Journal of Bridge Engineering, 2022, 27(5): 04022019

20. Zhu A, Li M, Zhu H P, Xu G, Xiao H, Ge H. Fatigue behaviour of orthotropic steel bridge decks with inner bulkheads. Journal of Constructional Steel Research, 2018, 146(7): 63−75
21. Li J P, Zhu Z W. Effects of full internal bulkheads on fatigue behaviors of orthotropic steel decks. Journal of Constructional Steel Research, 2022, 196: 107400
22. Xiang Z, Zhu Z W. Fatigue behavior of orthotropic composite bridge decks without cutout at rib-to-floorbeam intersection. Journal of Constructional Steel Research, 2018, 146(7): 63−75
23. Tai M, Arima Y, Shimozato T. Fatigue strength enhancement by structural modification of transverse to longitudinal rib connections in orthotropic steel decks with open ribs. Engineering Failure Analysis, 2020, 117: 104954
24. He X, Wu C, Wang R, Wei L, Jiang C. Experimental study on buckling behavior of orthotropic steel deck with slender open ribs for large span suspension bridges. Journal of Constructional Steel Research, 2023, 201: 107681
25. Zhang Q H, Liu Y, Bao Y, Jia D, Bu Y, Li Q. Fatigue performance of orthotropic steel−concrete composite deck with large-size longitudinal U-shape ribs. Engineering Structures, 2017, 150(11): 864−874
26. Shao X D, Yi D T, Huang Z Y, Zhao H, Chen B, Liu M. Basic performance of the composite deck system composed of orthotropic steel deck and ultrathin RPC layer. Journal of Bridge Engineering, 2013, 18(5): 417−428
27. Ding N, Shao X D. Study on fatigue performance of light-weighted composite bridge deck. China Civil Engineering Journal, 2015, 48(1): 74−81
28. Zhang S H, Shao X D, Cao J H, Cui J, Hu J, Deng L. Fatigue performance of a lightweight composite bridge deck with open ribs. Journal of Bridge Engineering, 2016, 21(7): 04016039
29. Pei B, Li L F, Shao X D, Wang L, Zeng Y. Field measurement and practical design of a lightweight composite bridge deck. Journal of Constructional Steel Research, 2018, 147(8): 564−574
30. Luo J, Shao X D, Fan W, Cao J, Deng S. Flexural cracking behavior and crack width predictions of composite (steel + UHPC) lightweight deck system. Engineering Structures, 2019, 194(9): 120−137
31. Luo J, Shao X D, Cao J H, Xiong M, Fan W. Transverse bending behavior of the steel–UHPC lightweight composite deck: Orthogonal test and analysis. Journal of Constructional Steel Research, 2019, 162(11): 105708
32. Wang Y, Shao X D, Chen J, Cao J, Deng S. UHPC-based strengthening technique for orthotropic steel decks with significant fatigue cracking issues. Journal of Constructional Steel Research, 2021, 176: 106393
33. Larrard F D, Sedran T. Optimization of ultra-high-performance concrete by the use of a packing model. Cement and Concrete Research, 1994, 24(6): 997−1009
34. Shen X J, Brühwiler E. Influence of local fiber distribution on tensile behavior of strain hardening UHPFRC using NDT and DIC. Cement and Concrete Research, 2020, 132: 106042
35. Feng J H, Shao X D, Qiu M H, Li H, Gao X, Huang Z. Reliability evaluation of flexural capacity design provision for UHPC beams reinforced with steel rebars/prestressing tendons. Engineering Structures, 2024, 300: 117160
36. Chen S, Huang Y, Gu P, Wang J Y. Experimental study on fatigue performance of UHPC-orthotropic steel composite deck. Thin-walled Structures, 2019, 142: 1−18
37. Xiang Z, Zhu Z W. Simulation study on fatigue behavior of wrap-around weld at rib-to-floorbeam joint in a steel–UHPC composite orthotropic bridge deck. Construction & Building Materials, 2021, 289(1): 123161
38. Yuan Y, Wu C, Jiang X. Experimental study on the fatigue behavior of the orthotropic steel deck rehabilitated by UHPC overlay. Journal of Constructional Steel Research, 2019, 157(6): 1−9
39. Wei C, Zhang Q H, Yang Z X, Li M, Cheng Z, Bao Y. Flexural cracking behavior of reinforced UHPC overlay in composite bridge deck with orthotropic steel deck under static and fatigue loads. Engineering Structures, 2022, 265(8): 114537
40. Pan W H, Fan J S, Nie J G, Hu J H, Cui J F. Experimental study on tensile behavior of wet joints in a prefabricated composite deck system composed of orthotropic steel deck and ultrathin reactive-powder concrete layer. Journal of Bridge Engineering, 2016, 21(10): 04016064
41. Shi Z C, Su Q, Kavoura F, Veljkovic M. Behavior of short-headed stud connectors in orthotropic steel–UHPC composite bridge deck under fatigue loading. International Journal of Fatigue, 2022, 160: 106845
42. Cao J H, Shao X D, Deng L, Gan Y. Static and fatigue behavior of short-headed studs embedded in a thin ultrahigh-performance concrete layer. Journal of Bridge Engineering, 2017, 22(5): 04017005
43. Qin S Q, Zhang J, Huang C L, Gao L, Bao Y. Fatigue performance evaluation of steel–UHPC composite orthotropic deck in a long-span cable-stayed bridge under in-service traffic. Engineering Structures, 2022, 254: 113875
44. Di J, Ruan X Z, Zhou X H, Wang J, Peng X. Fatigue assessment of orthotropic steel bridge decks based on strain monitoring data. Engineering Structures, 2021, 228: 111437
45. JTG D64-2015. Specifications of Design of Highway Steel Bridge. Beijing: Ministry of Transport of the People’s Republic of China, 2015
46. Hobbacher A F. Recommendations for Fatigue Design of Welded Joints and Components. 2nd ed. Villepinte: International Institute of Welding, 2016
47. En 1993-1-9. Eurocode 3: Design of Steel Structures-Part 1–9: Fatigue. Brussels: European Committee for Standardization, 2005